Heat capacity and structural transition effect in polycrystalline kesterite

Cédric Bourgès[1,*], Andrei Novitskii[2], Makoto Tachibana[2], Naoki Sato[2], and Takao Mori[2,3]

[1] *International Center for Young Scientists (ICYS), National Institute for Materials Science (NIMS), Namiki 1-1, Tsukuba, Ibaraki 305-0044, Japan*
[2]*MANA, National Institute for Materials Science (NIMS), Namiki 1-1, Tsukuba, Ibaraki 305-0044, Japan*
[3]*Graduate School of Pure and Applied Sciences, University of Tsukuba, Tennoudai 1-1-1, Tsukuba, Ibaraki 305-8577, Japan*

Corresponding Author: BOURGES.Cedric@nims.go.jp

Keywords: Kesterite, Heat Capacity, Cu_2ZnSnS_4,

Samples synthesis method:

The raw powders were synthesized by mixing 5 g of the stoichiometric ratio of the elemental Copper (≥ 99.9%, powder, 75 μm pass, Alfa Aesar), Zinc (99.9%, Powder, 75 – 150 μm, Alfa Aesar), Tin (99.8%, powder, < 45 μm, Alfa Aesar) and Sulfur (≥ 99.99%, Flake, Alfa Aesar) in a stainless-steel grinding vial containing two 10 mmØ and four 5 mmØ stainless steel balls for 3 h in a SPEX 8000D mixer/mill (Cole-Parmer, USA). The resulting powder was sintered by Spark Plasma Sintering (SPS-1080 – SPS Syntex Inc., Japan) in a 10 mm diameter graphite die under a partial vacuum atmosphere at 773 K for 15 min with a heating/cooling rate of 50 K/min and a constant uniaxial load of 50 MPa.

Detail of the Cp measurement:

The temperature-dependent heat capacity C_p studied from 315 to 773 K, was determined by Differential Scanning Calorimetry (DSC 404 Netzsch, Germany) measurement system using the ratio method and a sapphire standard reference (m_{ref} = 40.9 mg) in Al crucibles ($m_{crucible} \approx 40$ mg). Two square plate samples of $x = 0$ ($m_{1\text{-}2}$ = 64 and 94 mg) and two plates samples of $x = 0.125$ ($m_{3\text{-}4}$ = 57 and 76 mg) has been measured knowing that the highest mass correspond to the experimental limitation. A pre-isothermal segment of 50 min has been observed before the dynamic segment between 315 K and 773 K realized with a heating rate of 5 K/min.

For the low temperature range from 2 to 305 K, C_p measurements were performed using a physical property measurement system (PPMS; Quantum Design, USA) employing a relaxation method. Apiezon N high vacuum grease was applied to provide sufficient thermal contact between the sample and the platform in the high-vacuum environment during the measurement. A two quasi-square plate samples of $x = 0$ (m_5 = 28.02 mg) and $x = 0.125$ (m_6 = 30.31 mg) have been measured in the above-mentioned temperature range.

Computational method:

The DFT calculations were performed using Quantum ESPRESSO (QE)[1,2] package with projector augmented wave pseudopotentials.[3] The generalized gradient approximation functional with Perdew-Burke-Ernzerhof parametrization (GGA-PBE)[4] was chosen for the exchange and correlation potentials. We applied the Hubbard U correction to the strongly correlated Cu 3*d*, Zn 3*d*, and Sn 4*d* orbitals. We chose U_{eff} (= $U - V$) values as 5.2 eV, 6.5 eV, and 6.5 eV for Cu, Zn, and Sn, respectively. Spin-orbit coupling was not considered in the present study. The conventional unit cell with tetragonal lattice containing 16 atoms was fully relaxed until the residual forces became less than 10^{-6} eV Å^{-1}. The cutoff energy of 130 Ry for the plane wave basis and 8 × 8 × 4 *k*-grid were used for the structure relaxation.
To extract the second order interatomic force constants (IFCs), we used finite difference method with a 4 × 4 × 2 supercell based on the fully relaxed conventional cell to create displacement-force datasets. The magnitude of atomic displacements was set at 0.01 Å for calculating the second order IFCs. The IFCs were obtained using Phonopy.[5–7] The atom-projected vibration density of states (DOS) was calculated from the second order IFC. Dielectric constant and Born effective charge were calculated in the perturbation

framework implemented in the QE package for correcting phonon frequencies considering long-range interaction. The specific heat at constant volume, C_v, was calculated from the full spectrum of phonon DOS. Volume dependence of phonon frequencies were calculated at seven volume points around the equilibrium volume V_0 ($0.97V_0$, $0.98V_0$, $0.99V_0$, V_0, $1.01V_0$, $1.02V_0$, $1.03V_0$), and thermodynamic functions were calculated based on quasi-harmonic approximation implemented in Phonopy. Then, the temperature dependence of C_p was calculated from the C_v and Gibbs free energy.

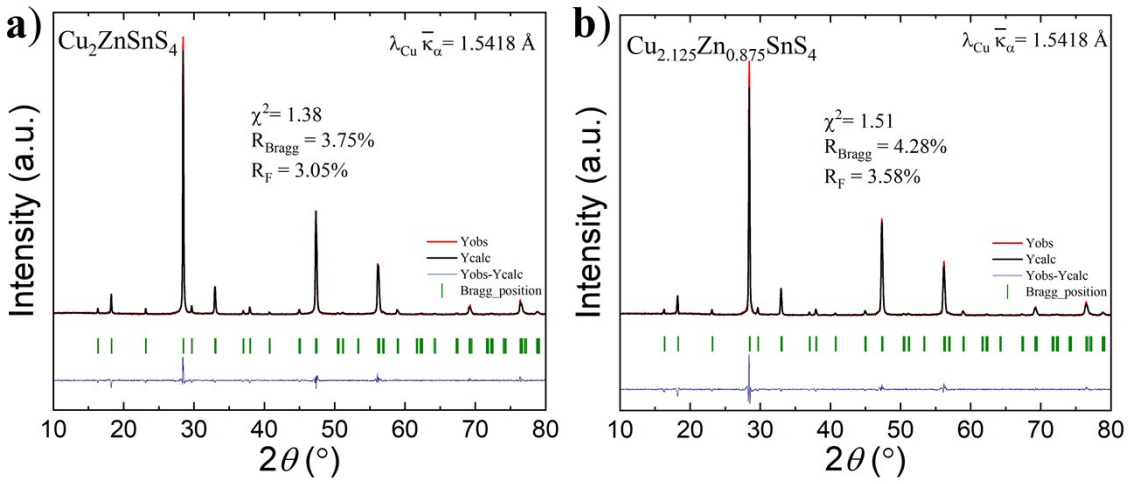

Figure S1. Room-temperature Rietveld refinement of the XRD patterns of the kesterite-$Cu_{2+x}Zn_{1-x}SnS_4$ for x = 0; 0.125

Table S2. Rietveld refinement parameter of the X-ray powder diffraction (XRPD) patterns of the CZTS SPSed samples.

$Cu_{2+x}Zn_{1-x}SnS_4$; $\lambda\kappa_\alpha$Cu = 1.5406 Å						
	***a* (Å)**	***c* (Å)**	***V* (Å^3)**	**χ2**	**R_{Bragg} (%)**	**R_F (%)**
***x* = 0**	5.432(1)	10.840(1)	319.77(5)	1.38	3.75	3.05
***x* = 0.125**	5.429(1)	10.841(1)	319.50(5)	1.51	4.28	3.58
Space group $I\bar{4}$ (n° 82)						
Atom	*X*	*Y*	*Z*	Occ.	B_{iso} (Å^2)	Mult.
Cu1	0.5	1	0.75	1	~0.6	2*c*
Cu2	0.5	0.5	0.5	1	~0.8	2*a*
Zn1	0	0.5	0.75	1	~0.8	2*d*
Sn1	0	1	0.5	1	~0.5	2*b*
S1	0.256	0.742	0.629	1	~0.5	8*g*

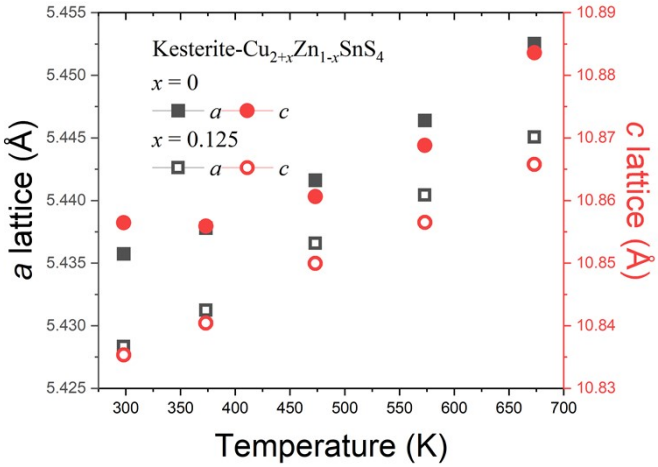

Figure S3. Temperature dependence of lattice parameters for the kesterite-$Cu_{2+x}Zn_{1-x}SnS_4$ with x = 0 and 0.125 obtained by pattern matching refinement of the HT-XRD.

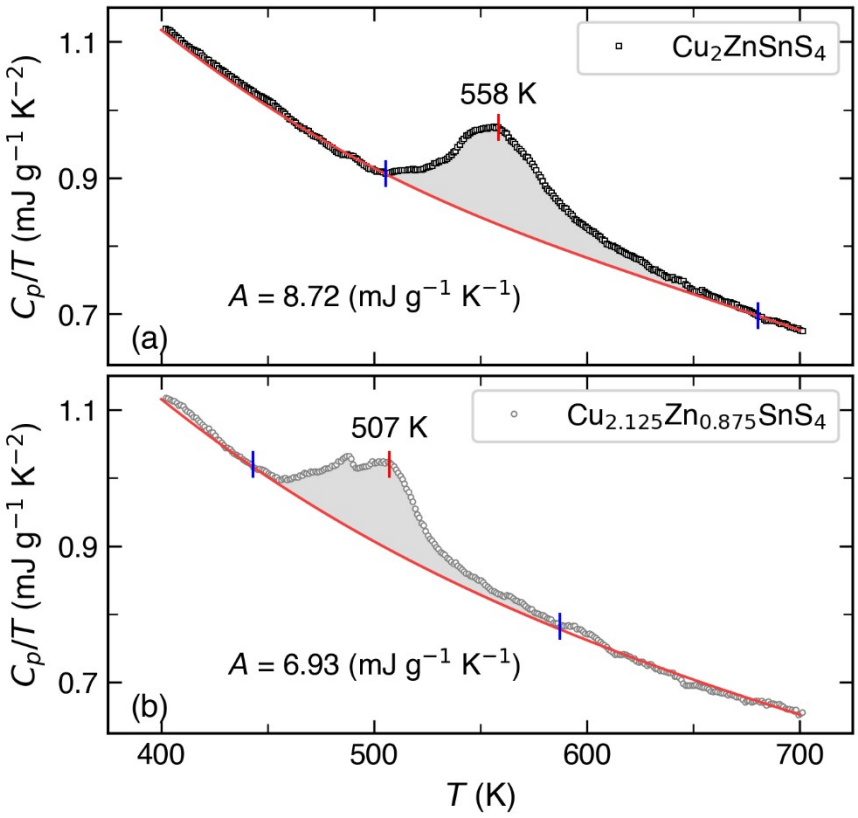

Figure S4. The heat capacity C_p of $Cu_{2+x}Zn_{1-x}SnS_4$ (a) x = 0, (b) x = 0.125) plotted as C_p/T function of T. Experimental data presented as gray and black empty symbols, while red lines, blue ticks, and grey area represent the background fit, the range limit and integral area.

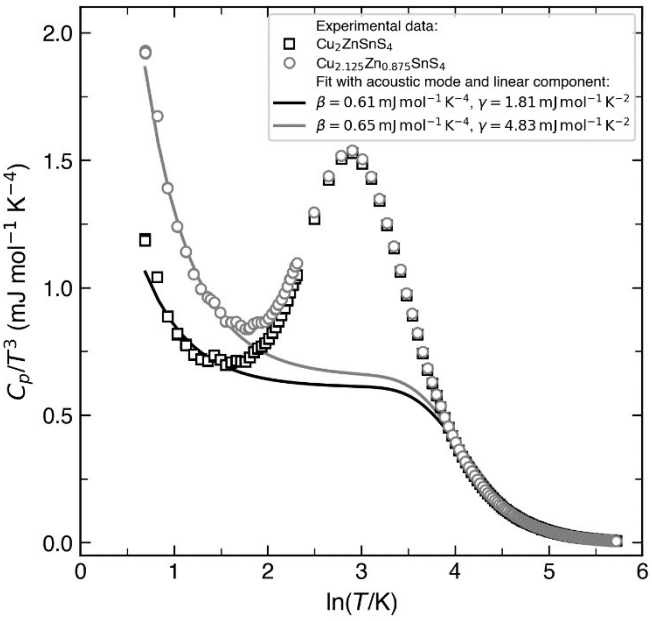

Figure S5. The heat capacity C_p of $Cu_{2+x}Zn_{1-x}SnS_4$ (x = 0, 0.125) plotted as C_p/T^3 versus lnT. Experimental data presented as gray and black empty symbols, while solid lines represent the Debye T^3 law with linear γT contribution: $C_p(T) = \beta T^3 + \gamma T$.

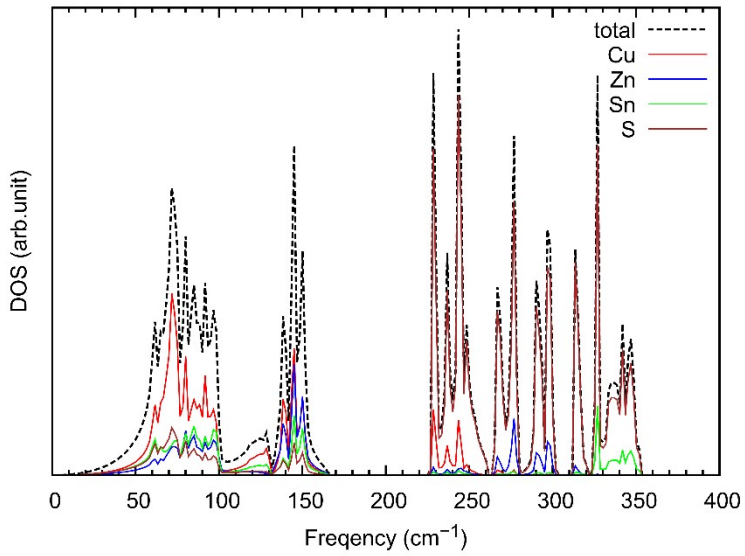

Figure S6. Atom-projected vibrational density of states (DOS) of kesterite proto structure Cu_2ZnSnS_4.

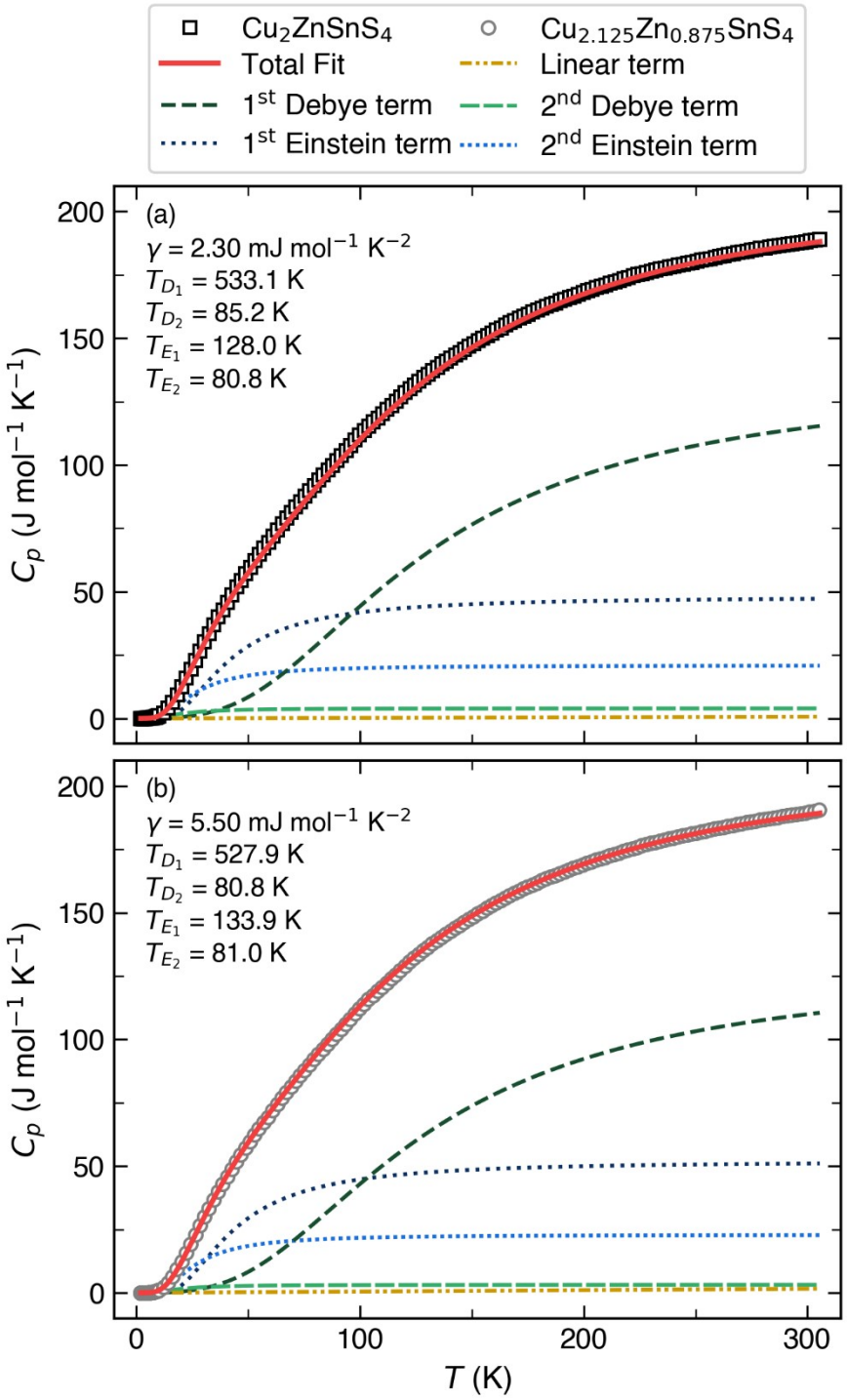

Figure S7. The heat capacity C_p of $Cu_{2+x}Zn_{1-x}SnS_4$ for (a)x = 0 and (b) x = 0.125 as a function of T from 2 to 300 K. Experimental data presented as gray and black empty symbols, while green dashed, blue dotted, and yellow dashed dotted lines represent Debye, Einstein, and linear contributions.

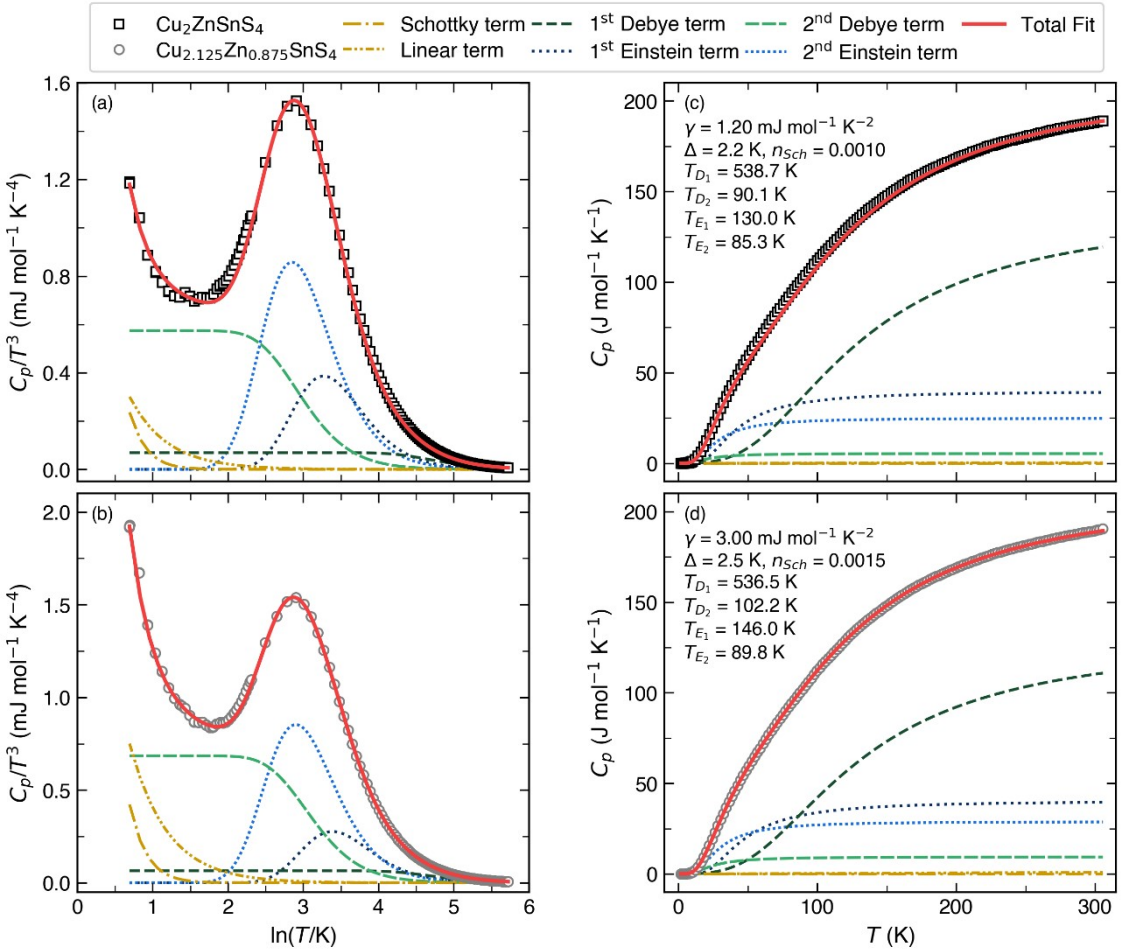

Figure S8. The heat capacity C_p of (a) Cu_2ZnSnS_4 and (b) $Cu_{2.125}Zn_{0.875}SnS_4$ plotted as C_p/T^3 versus lnT, (c) Cu_2ZnSnS_4 and (b) $Cu_{2.125}Zn_{0.875}SnS_4$ plotted as C_p versus T Experimental data presented as gray and black empty symbols, while green dashed, blue dotted, and yellow dashed dotted lines represent Debye, Einstein, and linear-Schottky contributions.

References:

1 P. Giannozzi, S. Baroni, N. Bonini, M. Calandra, R. Car, C. Cavazzoni, D. Ceresoli, G. L. Chiarotti, M. Cococcioni, I. Dabo, A. Dal Corso, S. de Gironcoli, S. Fabris, G. Fratesi, R. Gebauer, U. Gerstmann, C. Gougoussis, A. Kokalj, M. Lazzeri, L. Martin-Samos, N. Marzari, F. Mauri, R. Mazzarello, S. Paolini, A. Pasquarello, L. Paulatto, C. Sbraccia, S. Scandolo, G. Sclauzero, A. P. Seitsonen, A. Smogunov, P. Umari and R. M. Wentzcovitch, *J. Phys. Cond. Matter*, 2009, **21**, 395502.

2 P. Giannozzi, O. Andreussi, T. Brumme, O. Bunau, M. Buongiorno Nardelli, M. Calandra, R. Car, C. Cavazzoni, D. Ceresoli, M. Cococcioni, N. Colonna, I. Carnimeo, A. Dal Corso, S. De Gironcoli, P. Delugas, R. A. Distasio, A. Ferretti, A. Floris, G. Fratesi, G. Fugallo, R. Gebauer, U. Gerstmann, F. Giustino, T. Gorni, J. Jia, M. Kawamura, H. Y. Ko, A. Kokalj, E. Kücükbenli, M. Lazzeri, M. Marsili, N. Marzari, F. Mauri, N. L. Nguyen, H. V. Nguyen, A. Otero-De-La-Roza, L. Paulatto, S. Poncé, D. Rocca, R. Sabatini, B. Santra, M. Schlipf, A. P. Seitsonen, A. Smogunov, I. Timrov, T. Thonhauser, P. Umari, N. Vast, X. Wu and S. Baroni, *J. Phys. Cond. Matter*, 2017, **29**, 465901.

3 P. E. Blöchl, *Phys. Rev. B*, 1994, **50**, 17953–17979.

4 J. P. Perdew, K. Burke and M. Ernzerhof, *Phys. Rev. Lett.*, 1996, **77**, 3865–3868.

5 A. Togo and I. Tanaka, *Scr. Mater.*, 2015, **108**, 1–5.

6 A. Togo, L. Chaput, T. Tadano and I. Tanaka, *J. Phys. Cond. Matter*, 2023, **35**, 353001.

7 A. Togo, *J. Phys. Soc. Japan*, 2023, **92**, 012001.